High-energy spectra of the atmospheric neutrinos: predictions and measurements

A. A. Kochanov,[1,2,*] A. D. Morozova,[2,3,†] T. S. Sinegovskaya,[4,‡] and S. I. Sinegovsky[2,5,§]

[1]*Institute of Solar-Terrestrial Physics,*
Siberian Branch, Russian Academy of Sciences, RU-664033, Irkutsk, Russia
[2]*Irkutsk State University, RU-664003 Irkutsk, Russia*
[3]*Dzhelepov Laboratory of Nuclear Problems,*
Joint Institute for Nuclear Research RU-141980 Dubna, Russia
[4]*Irkutsk State Transport University, RU-664074, Irkutsk, Russia*
[5]*Dzhelepov Laboratory of Nuclear Problems,*
Joint Institute for Nuclear Research, RU-141980 Dubna, Russia
(Dated: October 4, 2021)

Statistical analysis is performed of the atmospheric neutrino flux models as compared with the data of Frejus, AMANDA-II, IceCube, ANTARES, and Super-Kamiokande experiments. The main objective is to characterize models of hadron-nucleus interactions from the point of view of the statistical significance of the atmospheric neutrino flux predictions compared to the measurements. The flux calculations were performed in the framework of the single computational scheme involving a set of hadronic models combined with parameterizations of the primary cosmic rays spectrum by Hillas & Gaisser and Zatsepin & Sokolskaya. The analysis showed satisfactory agreement of the conventional ν_μ flux calculations with the measurements. The prompt neutrinos conrtibution obtained with a set of charm production models (QGSM, SIBYLL 2.3c, PROSA, GRRST, BEJKRSS, and GM-VFNS) is statistically negligible in the energy range covered by the neutrino telescopes.

I. INTRODUCTION

Decays of pions, kaons, and charmed particles produced in cosmic rays interactions with the Earth atmosphere generate high-energy neutrinos which form an unavoidable background for detecting astrophysical neutrinos. To date, the atmospheric muon and the electron neutrino spectra are measured in Frejus [1], AMANDA-II [2, 3], ANTARES [4, 5], IceCube [6–11], and Super-Kamiokande [12] experiments within the energy range ~ 10 GeV through 600 TeV.

By the time, when detector AMANDA at the South Pole was constructed, the Monte Carlo calculations of the atmospheric neutrinos (AN) spectra had been performed for the neutrino energies of no more than 10 TeV [13–15]. Later on, these results were used to reconstruct the events in the IceCube [8] and Super-Kamiokande experiments.

The reference model for the AN spectra in IceCube is based on the Monte Carlo calculation (for $E \leq 10$ TeV) [14]. This model was extrapolated to energies beyond 10 TeV, taking into consideration the knee of the primary cosmic ray spectrum with normalizing corrections depending on the energy [9]. Thus, there is a necessity of a consistent scheme for AN spectra calculations over a wide neutrino energy range. The scheme validation should be done via a thorough comparison with the experimental data.

Here we apply the $Z(E, h)$ method [16–19], developed to solve the high-energy atmospheric hadron cascade equations and to compute the atmospheric muon and neutrino fluxes. The $Z(E, h)$ method enables us to compute atmospheric fluxes of hadrons, muons, and neutrinos for a non-power-law spectrum of cosmic rays, the non-scaling behavior of inclusive cross sections, and rising cross sections for inelastic hadron-nucleus collisions. The method have been tested [18, 20] by comparing the calculated fluxes of high energy atmospheric hadrons and muons with the data of the past decade experiments. The atmospheric muon spectra at various zenith angles have been thoroughly examined for wide energy range [18, 21, 22]. The method enables one to estimate directly the effect of the primary cosmic ray spectrum and the hadronic interactions models on the absolute values of muon and neutrino fluxes without recourse to any normalizing factors.

In this study, we analyze statistically the predicted atmospheric neutrinos spectra as compared with measured ones, by using standard χ^2 criterion. This work continues and extends the topic touched upon in the conference talk [23].

II. SPECTRA OF ATMOSPHERIC NEUTRINOS

The atmospheric neutrinos comprise two components, "soft" and "hard", clearly distinguishable in zenith-angle distributions and energy spectra. The anisotropic component originated from decays of pions and kaons has

*Electronic address: kochanov@iszf.irk.ru
†Electronic address: anniemor@jinr.ru
‡Electronic address: tanya@api.isu.ru
§Electronic address: sinegovsky@jinr.ru

a softer spectrum ("conventional" neutrinos, CN). The quasi-isotropic flux of neutrinos produced at higher energies, mainly in decays of charmed hadrons ($D^\pm$, D^0, $\overline{D}^0$, Λ_c^+), features a harder spectrum ("prompt" neutrinos, PN). Due to a very short lifetime of charmed particles ($\sim 10^{-12} - 10^{-13}$ s), they decay close to their production point. This fact implies that the spectral index of the PN flux is a unit harder than the CN one. Calculations of the PN flux are most uncertain due to wide spread predictions of the charm production models (see for example [24]). Until now, the prompt component of the atmospheric neutrinos has not been identified in experiments. A common expectation is that so-called "crossing energy" for prompt muon neutrinos is rather close to PeV.

A. Conventional neutrinos

Conventional atmospheric neutrinos within ~ 100 GeV to 10 PeV, produced in decays of $\pi^\pm$, $K^\pm$, K_L^0, and K_S^0 mesons were discussed in [19, 25–29]. The neutrino spectra were computed for a set of hadron-nucleus interaction models QGSJET-II-03 [30–32], SIBYLL 2.1 [33], and model by Kimel & Mokhov (KM) [34, 35], which are used also in Monte Carlo simulations of extensive air showers produced by cosmic rays. We apply two cosmic ray spectrum models by Zatsepin and Sokolskaya (ZS) [36] and by Hillas and Gaisser [37] (chosen was the H3a version for mixed composition of the extragalactic component). The ZS comprises contributions from three classes of Galaxy cosmic rays sources: isolated SNe exploding into a random interstellar medium (ISM), high mass SNe exploding into a dense ISM (OB associations), and weak sources associated with novae explosions. The ZS spectrum supported by direct measurements of ATIC-2 experiment [38, 39] within 10 GeV–50 TeV serves, indeed, as an extrapolation of the CR spectrum beyond PeV (up to 100 PeV), and thefore the calculated neutrino flux in case of ZS spectrum should be restricted to $E_\nu < 10$ PeV.

The Hillas and Gaisser model [37] includes three classes of sources: supernovae remnants in the Galaxy, Galaxy high-energy sources of unknown origin (that contribute to the cosmic ray flux between the knee (3 PeV) and the ankle (4 EeV)), and extragalactic astrophysical objects (Active Galactic Nuclei, sources of the gamma-ray bursts, and others). The composite spectrum is formed of five nuclei groups (p, He, CNO, Mg-Si, and Mn-Fe). Each of the three populations accelerates five nuclei groups, whose spectrum cuts off at a characteristic rigidity.

Figures 1, 2 present the coventional neutrinos fluxes, calculated with the hadronic models (QGSJET-II-03, SIBYLL 2.1, and KM), together with the experimental data. The main content of these figures is the comparison of calculated CN flux with experiments. However, the curves of the prompt neutrino spectra also shown in figures to exhibit distinctions between CN and PN fluxes. Hereinafter, ν_μ and ν_e designate the sums of neutrinos and antineutrinos, $\nu_\mu + \overline{\nu}_\mu$ and $\nu_e + \overline{\nu}_e$, respectively.

B. Prompt neutrinos

1. Charm production models

In this study, we use the prompt neutrino (PN) contributions obtained with the charm production models: QGSM [24], SIBYLL 2.3c [40], PROSA Collaboration [41, 42], GRRST [43], BEJKRSS [44], and GM-VFNS [45].

The non-perturbative quark-gluon string model (QGSM) was developed [46, 47] to describe the soft and semihard hadronic processes at high energies. It has been applied to successfully describe the meson and baryon production in hadron-nucleon collisions. The QGSM was one of the first models to estimate the atmospheric prompt muon and neutrino fluxes [48–50]. Here, we use the results of the prompt muon neutrino flux calculations at 1 TeV – 100 PeV performed with the updated QGSM [24]. Prameters of the updated QGSM were examined by comparing the calculated cross sections for the charmed meson production with the measurements in the LHCb and ALICE experiments. Although the LHCb does not enable an unique choice of the QGSM parameters, the intercept of the Regge trajectory $\alpha_\psi(0) = -2.2$ appears a more preferable value versus $\alpha_\psi(0) = 0$. Another QGSM free parameter is the coefficient a_1 providing an unified description for the $x \to 0$ and $x \to 1$ kinematic regions in the case of the leading fragmentation. There are no clear arguments for choosing a_1, and we calculate the PN flux for this parameter, varying from $a_1 = 2$ and $a_1 = 30$ (shaded band in Figure 3).

The SIBYLL 2.3c [40] was used to calculate the PN spectra based on numerical solver for the system of the coupled cascade equations (Matrix Cascade Equations, MCE_Q-method) [51, 52]. The model for charm quark production is based on the LO QCD computations and the probability for the replacing s quarks by c ones in the fragmentation process.

The PROSA collaboration [41, 42] has presented the thorough study of the atmospheric prompt neutrino problem with usage of the PROSA Monte Carlo event generator. The PROSA computaions were based on the LHCb and ALICE measurements of the charmed hadron production and improved constraints on the paron distribution functions (PDFs) in NLO QCD analysis using DIS and pp collision data. The prompt ν_μ spectrum was obtained through the atmospheric cascade equations that describe the production and decay of secondary particles arising from cosmic ray interactions which produce finally the atmospheric muons and neutrinos. The cascade equations admit approximate solutions in the z-moment approach with use of the superposition model for pA and AA interactions. The z-moments were calculated with the PROSA PDFs at the next-to-leading order (NLO) perturbative QCD (pQCD) in the fixed/variable flavour number schemes (FFNS/VFNS) consistent with the LHCb, ALICE and HERA measurements of charmed and beauty-flavoured hadrons. It was shown that PDF

uncertainties lead to the smaller flux uncertainty with respect to those arising from a choice of the QCD renormalization and factorization scales. The variations of phenomenological parameters of the charm fragmentation functions, as well as the choice of the cosmic ray model (the CR compossition and spectrum) have also considerable impact on the flux uncertainty.

The PN spectra predicted with GRRST model [43] are based on the Monte Carlo event generator using the z-moment approach to simulate of particles propagation and decays in the framework of NLO pQCD calculations through the same set of high energy charmed hadrons as in the PROSA approach. Cross sections of charmed particles production are obtained with the PDFs integrated the measurements of charm production at the LHCb experiment. Uncertainties of calculations are defined by the "scale uncertainties" of the NLO perturbative QCD and are reduced by NNLO calculations. Also the uncertainties of gluon PDF at small x variable make a sizable contribution to the total errors of predicted PN, especially at $E_\nu > 1$ PeV.

The PN flux predicted with BEJKRSS model [44] was evaluated using the scheme for calculation of the charm production cross section, which comprises the NLO pQCD computations, the k_T factorization approach with the low x resummation, and the color dipole model comprising the gluon saturation. The QCD parameters were chosen to provide the best fit of the heavy quark production cross sections measured in RHIC and LHCb experiments. The latest version of BEJKRSS model incorporates nuclear effects in the target PDFs, which usually are neglected in the perturbative approach, although the nuclear shadowing effects may be considerable at very low x region. It was found that the reduction of the neutrino flux due to nuclear efects varies from 10% to 50% at the highest energies, depending on the used scheme.

The general-mass variable flavour number scheme (GM-VFNS) model [45] bases on the NLO pQCD approach in which the matrix elements for the charm hadroproduction of light and heavy partons are combined with a set of fragmentation functions to describe the hadronization process (transition from partons to charmed hadrons). The scheme involves only one massive heavy quark m_Q, other quarks are massless. The GM-VFNS appropriates different approaches for calculation of cross sections: the FFNS scheme uses in low and intermediate p_T, and zero mass VFNS framework does in high regions of p_T. The validity of the approach has been cross-checked by comparisons with data measured with the LHCb experiment. Uncertainty of predicted PN spectra arises from renormalization scale around central value (with a permanent level of half of order of PN magnitude) and from the PDF uncertainty, which rapidly grows to two and a half orders of magnitude for very high energies.

2. PN flux predictions

This work analysis concerns only atmospheric muon and electron neutrinos, because tau neutrinos substantially are the prompt ones (originate from $D_s^\pm$ and τ decays) and they are suppressed by one order of magnitude [40].

The PN spectra are plotted in Figs. 3, the calculations are performed for the H3a spectrum of primary cosmic rays. Prompt electron neutrinos dominate over the conventional ones at energies beyond 50 TeV, while the prompt muon neutrinos become the dominant component at the PeV scale. The PN energy spectra are calculated for the vertical direction (no averaging over zenith angles). The isotropic approximation provides a reasonable estimate at energies below 3 PeV where the PN flux weakly depends on the zenith angle. The directions around the vertical are most suitable to reveal PN neutrinos because of the best PN/CN flux ratio. The green band shows the QGSM calculation uncertainty relating to varying free parameter a_1, that provides a unified description for the kinematic regions $x \to 0$ and $x \to 1$ in the case, when the valence quarks participate in fragmentation [24]. We do not show uncertainties of the spectra computed by the PROSA [41] which absorb those of the rest models. All χ^2 values are obtained for the central values of PN predictions.

These models predictions display the spread of the prompt neutrino flux obtained for the H3a spectrum of cosmic rays, i.e. these models mark the approximate range of the PN contribution calculated with H3a spectrum (the use of the ZS spectrum weakly affects the range). The PN fluxes obtained with QGSM [24], PROSA [41] are very close to each other within a wide energy range (Fig. 3). The SIBYLL 2.3c [40] also predicts the PN flux rather close to that of PROSA and QGSM. Shaded area in Figure 3 shows the spread of model predictions for the median "crossing energy", i.e. the energy, above which the atmospheric neutrino flux is dominated by the PN component (see also Table IV). All the fluxes are calculated for the H3a model of primary cosmic rays spectrum.

III. EXPERIMENTAL DATA

The reconstructed neutrino energy spectra are derived from the neutrino telescopes with large statistical and systematical errors due to the restricted set of data and necessity to resort to sophisticated technique of handling the neutrino events. The total errors of the ν_μ and ν_e spectra measured in the Fréjus experiment [1] at zenith angles $90^\circ < \theta < 180^\circ$, vary from $\sim 26\%$ to $\sim 55\%$ in low and high neutrino energies within the range of $0.25 < E_\nu \lesssim 10^3$ GeV.

Preliminary results of the AMANDA-II experiment obtained at 90% CL without zenith angles cuts were reported in 2009 [2] (grey band in the Figure 1 (a)). In the
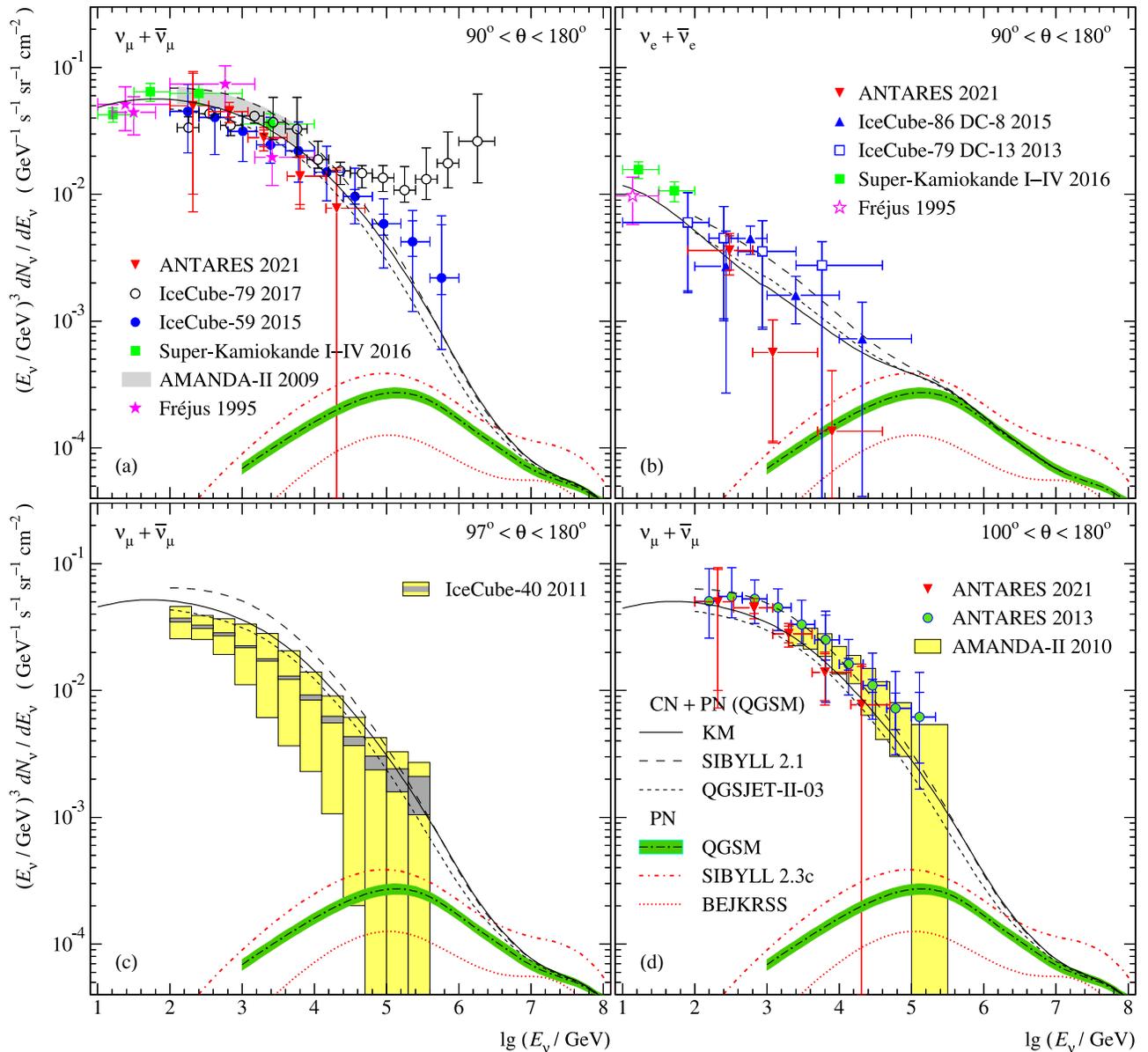
Figure 1: Calculated atmospheric neutrino spectra (scaled by E_ν^3) averaged over zenith angles, ν_μ (a), (c), (d), and ν_e (b) compared to the data of experiments: Fréjus [1], AMANDA-II [2, 3], ANTARES [4, 5], IceCube-40 [6], IceCube-59 [9], IceCube-79 [7], IceCube-86 [10], and Super-Kamiokande I–IV [12]. Error bars correspond to the uncertainties, including all statistical and systematic errors. Grey band in panel (a) indicates the 90% CL from the forward-folding analysis of AMANDA-II 2009 [2]. The total errors (yellow rectangles) and statistical ones (dark rectangles) for the IceCube-40 data and AMANDA-II 2010 [3] are shown in panels (c) and (d). The spectra are calculated with H3a parameterization of the cosmic rays spectrum [37] for hadronic models KM (solid lines), SIBYLL 2.1 (dashed), and QGSJET-II-03 (short dashed). Also shown are the PN spectra calculated with QGSM [24], SIBYLL 2.3c [40], and BEJKRSS [44].

final AMANDA-II data [3], muon tracks with $\theta < 100^\circ$ are removed from the analysis to minimize the atmospheric muon contamination of the neutrino sample. The final sample contains 2972 neutrino-induced events. The statistical errors of the ν_μ spectra measured with the AMANDA-II (for 807 days between 2000 and 2003) for $100^\circ < \theta < 180^\circ$ are obtained of 18% for low and 60% for high neutrino energies. The systematical errors are 16% within the entire energy range, $10^3 \lesssim E_\nu \lesssim 10^6$ GeV

(yellow rectangles in Figure 1 (d)).

The total errors of the neutrino spectra reconstructed in the ANTARES 2013 [4] (855 days in 2007–2011) for energies $10^2 < E_\nu \lesssim 10^6$ GeV are 30% and 125% for low and high energies, respectively. To suppress background events induced by atmospheric muons, zenith angles were restricted to the range $100^\circ < \theta < 180^\circ$.

The recent data published by the ANTARES Collaboration in 2021 [5] were collected in the period 2007–2017
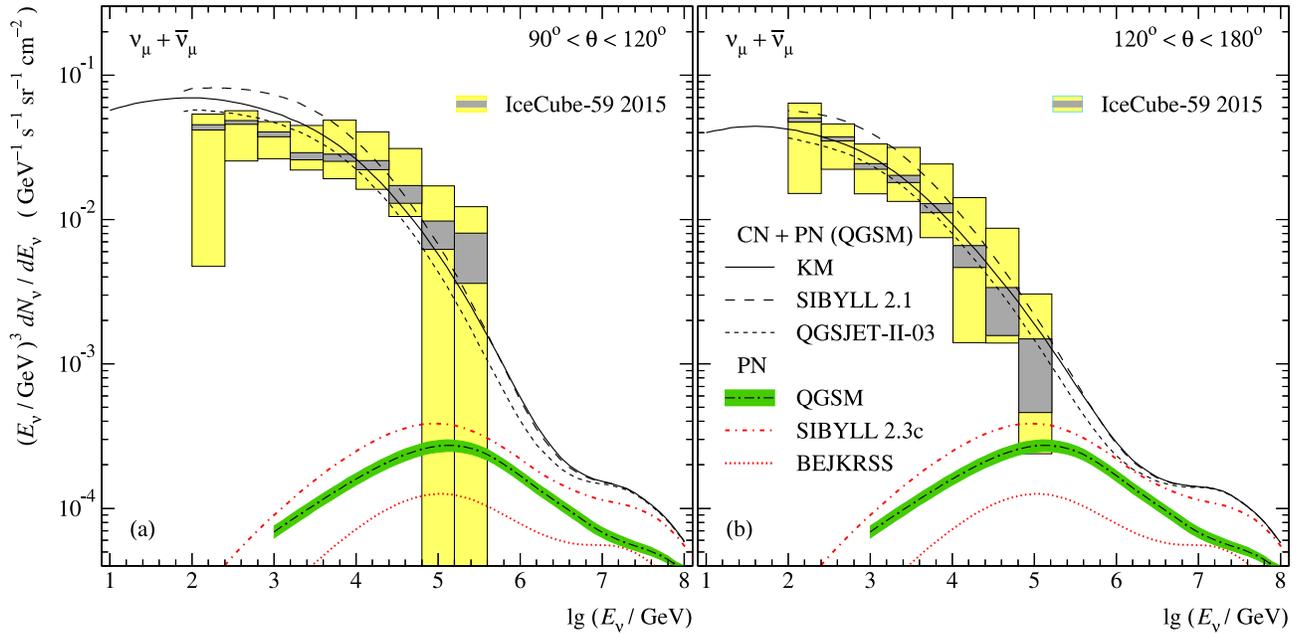
Figure 2: Calculated energy spectra of the atmospheric muon neutrinos averaged over $90^{\circ} < \theta < 120^{\circ}$ (a), and $120^{\circ} < \theta < 180^{\circ}$ (b) in comparison with the IceCube-59 data [9]. The total and statistical measurement errors are shown as light and dark shaded rectangles. Notations of experimental errors and theoretical predictions of the CN and PN fluxes are the same as in Figure 1.
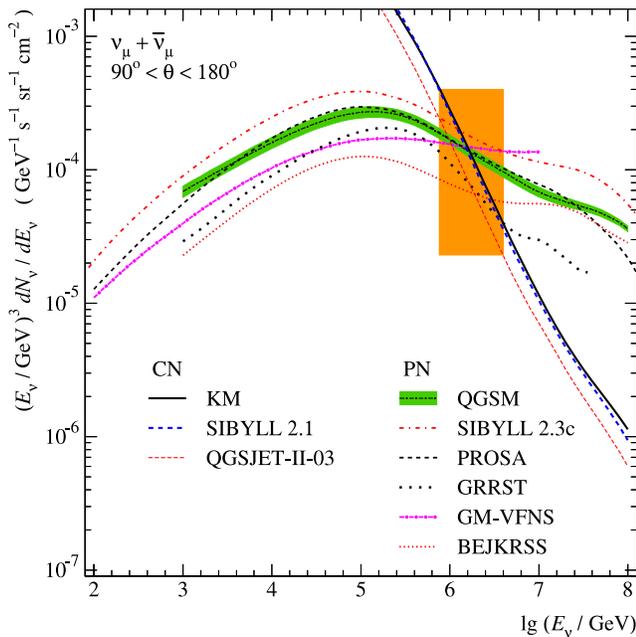

Figure 3: Prompt ν_{μ} spectra (scaled by factor E_{ν}^3) at $\theta = 0^{\circ}$ calculated with charm production models QGSM [24], SIBYLL 2.3c [40], GRRST [43], BEJKRSS [44], GM-VFNS [45], and PROSA [41]. The CN spectra averaged over zenith angles are also shown. The shaded rectangle displays the "crossing energy" range predicted with different PN flux models. All the fluxes are calculated for the H3a model of primary cosmic rays spectrum.

in the energy range between ~ 100 GeV and ~ 50 TeV (5 bins for ν_{μ} and 3 bins for ν_e); the zenith angles interval is $90^{\circ} < \theta < 180^{\circ}$. The statistical uncertainties of the ANTARES 2021 reconstruction are rather large: $10\% - 100\%$ (ν_{μ}) and $30\% - 200\%$ (ν_e). During of 3012 days of the livetime, about 130 ν_e and 850 ν_{μ} events were reconstructed in the instrumented volume of ANTARES detector.

The density of ANTARES optical modules is insufficient to reconstruct a considerable number of events induced by neutrinos at energies below 100 GeV. The low statistics of the ν_e events prevents from testing charm production models above tens of TeV, i.e. in the energy range, where one could expect an appreciable contribution of the prompt electron neutrinos. The energy estimate for the semi-contained events relative to the through-going ones reduces the overall uncertainty of the measured flux as compared with ANTARES 2013 measurements. The ANTARES 2021 ν_{μ} flux is close to that of IceCube-40 (2011) and IceCube-59 (2015), and $20\% - 25\%$ below the flux reported in the ANTARES 2013 measurement.

The total experimental errors of the neutrino spectra reconstructed in the Super-Kamiokande [12] (operated intermittently since 1996, but the data sets used in this paper include the data until 2015) vary from 15% to 19% (ν_e) and $15\% - 21\%$ (ν_{μ}) in the energy range $0.25 < E_{\nu} < 10^4$ GeV.

In the period $2008 - 2009$, the IceCube detector was operated in the 40-strings configuration [6]. The results of the measurements were presented for three zenith an-

gles intervals: $97^{\text{o}} < \theta < 124^{\text{o}}$, $124^{\text{o}} < \theta < 180^{\text{o}}$, and $97^{\text{o}} < \theta < 180^{\text{o}}$ (joint interval). The authors of the experiment have published the errors only for the joint interval. The total errors for the joint analysis were estimated from 21% to 158% for low and high energies in the range $10^2 < E_\nu \lesssim 10^6$ GeV.

The first data on the atmospheric ν_e flux in TeV energy range were obtained in $2010 - 2011$ using the DeepCore infill array in the IceCube-79 (the 79-strings configuration) [7]. DeepCore included the six specialized strings and the seven adjacent standard IceCube strings (DeepCore-13) and allowed reducing the energy threshold to ~ 10 GeV. Four data points of the reconstructed atmospheric ν_e spectrum were obtained from a selected data sample of 496 ± 66 (stat) ± 88 (syst) cascade events observed in 281 days of data. They included ν_e charge currrent interactions and neutral current interactions of neutrinos of all flavors. The experimental errors of measured ν_e spectra are from 54% to 100% in the energy range 80 GeV – 6 TeV.

In $2011 - 2012$, a new IceCube analysis of the ν_e spectrum was based on the data taken for $97^{\text{o}} < \theta < 180^{\text{o}}$ with the full 86-string configuration during 332.3 days of livetime [10]. The total errors of data are estimated as $25\% - 94\%$ for energies $10^2 < E_\nu \lesssim 10^5$ GeV. Whereas the information on zenith angles cuts is not entirely clear, we do not apply any cuts in our analysis. The IceCube-59 experimental data for ν_μ were taken in $2009 - 2010$ with the 59-string configuration of the detector [9]. Like in the IceCube-40, the analysis of events addresses three intervals of zenith angles, $90^{\text{o}} < \theta < 120^{\text{o}}$, $120^{\text{o}} < \theta < 180^{\text{o}}$, and $90^{\text{o}} < \theta < 180^{\text{o}}$. The total errors are estimated from $\sim 25\%$ to $\sim 250\%$ for energies $10^2 < E_\nu \lesssim 10^6$ GeV. We do not use the IceCube-79 data [11] in our analysis, because they contain uncertain admixture of astrophysical neutrinos.

Thus, the total data set for the statistical analysis for ν_μ spectra contains 54 data points measured with Fréjus (4 points), AMANDA-II (9 points), IceCube-40 (12 points), ANTARES 2013 (10 points), ANTARES 2021 (5 points), Super-Kamiokande (4 points), and IceCube-59 (10 points) at zenith angles in the interval $90^{\text{o}} < \theta < 180^{\text{o}}$. The set for the analysis of ν_e spectra includes 11 data points obtained in Super-Kamiokande [12], IceCube-79 [7], IceCube-86, and ANTARES 2021 [5]. Figures 1 and 2 show the measured and predicted spectra calculated with the models tested in our analysis. Figure 1(b) shows the experimental data for ν_e spectra measured in Fréjus 1995 [1], Super-Kamiokande [12] for zenith angles $90^{\text{o}} < \theta < 180^{\text{o}}$ along with the predicted spectra averaged over the narrowed angle interval, $97^{\text{o}} < \theta < 180^{\text{o}}$.

IV. STATISTICAL ANALYSIS

A set of n independent measurements Φ_i (energy spectrum) at points E_i (energy) is considered as Gaussian distributed with the mean $\mu(E_i; \vec{\alpha}, \vec{\beta})$ and known variance σ_i^2. The goal of the statistical analysis is to construct estimators for the unknown parameters $\vec{\alpha}, \vec{\beta}$. In our case, $\vec{\alpha}$ stands for hadronic models ($\alpha_j, j = 1, 2, 3$) and $\vec{\beta}$ labels models of cosmic ray spectrum ($\beta_k, k = 1, 2$). That is, index j implies a hadronic interaction model KM, QGSJET-II-03 and SIBYLL 2.1, and j marks CR models H3a and ZS.

For the statistical analysis [53, 54] we use χ^2 values

$$\chi^2(\vec{\alpha}, \vec{\beta}) = \sum_{i=1}^{\text{ndf}} \frac{\left(\Phi_i^{\text{exp}} - < \phi_i^{(\vec{\alpha}, \vec{\beta})} > \right)^2}{(\delta \Phi_i^{\text{exp}})^2}, \qquad (1)$$

where Φ_i^{exp} is the detected neutrino flux for i-th energy bin; $\phi_i^{(\vec{\alpha}, \vec{\beta})}$ is the calculated one for the chosen flux model (j, k); ndf is the number of the data bins (data points) index i enumerates the measured mean values E_i; $\delta \Phi_i^{\text{exp}}$ designates experimental errors (considering the systematic and statistical uncertainties). For each bin $\Phi(E_\nu) \equiv < dN_\nu/dE_\nu >_\theta$ denotes the differential neutrino flux (the energy spectrum) averaged over zenith angles. The predicted neutrino flux was averaged over energy in the i-th bin:

$$< \phi^{(\vec{\alpha}, \vec{\beta})}(\bar{E}_i) > = \frac{1}{\Delta E_i} \int_{E_i}^{E_{i+1}} \phi^{(\vec{\alpha}, \vec{\beta})}(E) dE. \qquad (2)$$

The quality of the overall fit can be judged from the global χ^2 divided by ndf. For each data set included in the analysis, a partial χ^2/ndf relating to single experiment is provided. The second column in Tables I–III presents χ^2/ndf obtained for the CN flux calculated with hadronic models, KM, QGSJET-II-03 and SIBYLL 2.1 (the flux model indices are dropped). Columns 3–5 are χ^2/ndf for the total neutrino flux, the conventional and the prompt one (CN+PN). Here, we show also results for the three charm production models QGSM, SIBYLL 2.3c, and BEJKRS (see Section II).

The partial and global χ^2/ndf values for the conventional muon neutrinos illustrate a satisfactory agreement among all the data sets (Tables I and II) except for AMANDA-II data. We may state, that the prompt muon neutrinos predicted with charm production models under study are statistically insignificant (Tables I, II). More optimistic picture is seen for the contribution of the prompt electron neutrinos with the SIBYLL 2.3c (4th column in Table III): for IceCube-86 experiment χ^2/ndf value is reduced by $\sim 8 - 10\%$. Unfortunately, total statistical significance of the ν_e data is not so high in our analysis due to restricted energy range.

V. RESULTS AND DISCUSSION

The obtained χ^2 values for each flux model and each experiment are shown in Tables I–III. Tables I and II

Table I: χ^2/ndf values for the predicted ν_μ spectra versus the experimental data. Calculations are made for the H3a and ZS (in brackets) cosmic ray spectrum.

Experiment, CN | PN models	χ^2 (CN)	χ^2 (CN+PN) QGSM	SIBYLL 2.3c	BEJKRSS
Fréjus 1995 [1], $E_\nu \lesssim 10^3$ GeV, $90^\circ < \theta < 180^\circ$				
KM		2.30/ 4 = 0.57 (2.77/ 4 = 0.69)		
QGSJET-II-03		0.23/ 2 = 0.11 (0.36/ 2 = 0.18)		
SIBYLL 2.1		6.78/ 2 = 3.39 (6.77/ 2 = 3.39)		
AMANDA-II 2010 [3], $10^3 \lesssim E_\nu \lesssim 10^6$ GeV, $100^\circ < \theta < 180^\circ$				
KM	21.4/ 9 = 2.38	20.5/ 9 = 2.28	20.1/ 9 = 2.23	21.0/ 9 = 2.33
	(29.1/ 9 = 3.23)	(28.1/ 9 = 3.12)	(27.6/ 9 = 3.07)	(28.6/ 9 = 3.18)
QGSJET-II-03	31.4/ 9 = 3.49	30.3/ 9 = 3.36	29.7/ 9 = 3.30	30.9/ 9 = 3.43
	(39.5/ 9 = 4.39)	(38.3/ 9 = 4.26)	(37.8/ 9 = 4.20)	(39.0/ 9 = 4.33)
SIBYLL 2.1	6.52/ 9 = 0.72	5.94/ 9 = 0.66	5.70/ 9 = 0.63	6.25/ 9 = 0.69
	(11.5/ 9 = 1.28)	(10.8/ 9 = 1.20)	(10.4/ 9 = 1.16)	(11.1/ 9 = 1.23)
IceCube-40 2011 [6], $10^2 < E_\nu \lesssim 10^6$ GeV, $97^\circ < \theta < 180^\circ$				
KM	0.78/12 = 0.06	0.87/12 = 0.07	0.92/12 = 0.08	0.82/12 = 0.07
	(0.70/12 = 0.06)	(0.72/12 = 0.06)	(0.75/12 = 0.06)	(0.71/12 = 0.06)
QGSJET-II-03	0.64/12 = 0.05	0.66/12 = 0.06	0.66/12 = 0.05	0.65/12 = 0.05
	(0.34/12 = 0.03)	(0.32/12 = 0.03)	(0.30/12 = 0.03)	(0.33/12 = 0.03)
SIBYLL 2.1	13.3/12 = 1.10	13.5/12 = 1.13	13.7/12 = 1.14	13.4/12 = 1.12
	(13.4/12 = 1.12)	(13.5/12 = 1.13)	(13.7/12 = 1.14)	(13.5/12 = 1.13)
ANTARES 2013 [4], $10^2 < E_\nu \lesssim 10^6$ GeV, $100^\circ < \theta < 180^\circ$				
KM	4.46/10 = 0.45	4.23/10 = 0.42	4.12/10 = 0.41	4.35/10 = 0.44
	(5.35/10 = 0.53)	(5.10/10 = 0.51)	(4.98/10 = 0.50)	(5.24/10 = 0.52)
QGSJET-II-03	7.17/10 = 0.72	6.90/10 = 0.69	6.77/10 = 0.68	7.05/10 = 0.70
	(8.19/10 = 0.82)	(7.91/10 = 0.79)	(7.77/10 = 0.78)	(8.06/10 = 0.81)
SIBYLL 2.1	1.58/10 = 0.16	1.43/10 = 0.14	1.37/10 = 0.14	1.51/10 = 0.15
	(2.35/10 = 0.23)	(2.18/10 = 0.22)	(2.10/10 = 0.21)	(2.27/10 = 0.23)
Super-Kamiokande I–IV 2016 [12], $E_\nu < 10^4$ GeV, $90^\circ < \theta < 180^\circ$				
KM		3.65/ 4 = 0.91 (4.29/ 4 = 1.07)		
QGSJET-II-03		4.01/ 2 = 2.01 (4.00/ 2 = 2.00)		
SIBYLL 2.1		1.38/ 2 = 0.69 (1.26/ 2 = 0.63)		
Combined data [1, 3, 4, 6, 12] $E_\nu \lesssim 10^6$ GeV				
KM	32.6/39 = 0.84	31.5/39 = 0.81	31.1/39 = 0.80	32.1/39 = 0.82
	(42.2/39 = 1.08)	(41.0/39 = 1.05)	(40.4/39 = 1.04)	(41.6/39 = 1.07)
QGSJET-II-03	43.4/35 = 1.24	42.1/35 = 1.20	41.3/35 = 1.18	42.8/35 = 1.22
	(52.4/35 = 1.50)	(50.9/35 = 1.45)	(50.2/35 = 1.43)	(51.7/35 = 1.48)
SIBYLL 2.1	29.6/35 = 0.84	29.1/35 = 0.83	29.0/35 = 0.83	29.3/35 = 0.84
	(35.3/35 = 1.01)	(34.6/35 = 0.99)	(34.4/35 = 0.98)	(35.0/35 = 1.00)

present the values of χ^2/ndf calculated for ν_μ, Table III does the same for ν_e spectra. The energy ranges and cuts for zenith angles are indicated for each experiment. Namely, Tables I and II show χ^2/ndf for ν_μ spectra by Fréjus [1], IceCube-40 2011 [6], IceCube-59 2015 [9], ANTARES 2013 [4], ANTARES 2021 [5], AMANDA-II 2010 [3], and Super-Kamiokande I–IV 2016 [12], as compared with the CN and CN+PN neutrino spectra predicted by QGSJET-II-03 [30–32], SIBYLL 2.1 [33], and KM [34, 35] for H3a and ZS (in brackets) cosmic ray spec-

tra. The CN spectra were averaged over the zenith angles according to the cuts provided by experimentalists.

The analysis is performed for five combinations: 1) ν_μ and ν_e separately for each experiment (ndf = $4 \div 12$); 2) the combined ν_μ data except for IceCube-59 and ANTARES 2021 (ndf = $35, 39$) (Table I); 3) combined all ν_μ data (ndf = $50, 54$)) (Table II); 4) the combined ANTARES 2013 and ANTARES 2021 ν_μ data (ndf = 15) (Table II); 5) the combined ν_e data of IceCube-79, IceCube-86, and ANTARES 2021 (Table III)

Table II: χ^2/ndf values obtained for predicted ν_μ spectra and measured ones in the IceCube and ANTARES experiments.

Experiment, CN | PN models	χ^2 (CN)	χ^2 (CN+PN) QGSM	SIBYLL 2.3c	BEJKRSS
IceCube-59 2015 [9], $10^2 < E_\nu \lesssim 10^6$ GeV, $90° < \theta < 120°$				
KM	11.0/ 9 = 1.22 (12.7/ 9 = 1.41)	10.9/ 9 = 1.22 (12.6/ 9 = 1.40)	11.0/ 9 = 1.22 (12.7/ 9 = 1.41)	10.9/ 9 = 1.21 (12.6/ 9 = 1.40)
QGSJET-II-03	4.60/ 9 = 0.51 (4.89/ 9 = 0.53)	4.52/ 9 = 0.50 (4.70/ 9 = 0.52)	4.51/ 9 = 0.50 (4.69/ 9 = 0.52)	4.56/ 9 = 0.51 (4.75/ 9 = 0.53)
SIBYLL 2.1	35.1/ 9 = 3.90 (36.2/ 9 = 4.02)	35.1/ 9 = 3.90 (36.2/ 9 = 4.02)	35.2/ 9 = 3.91 (36.3/ 9 = 4.03)	35.1/ 9 = 3.90 (36.2/ 9 = 4.02)
IceCube-59 2015 [9], $10^2 < E_\nu \lesssim 10^6$ GeV, $120° < \theta < 180°$				
KM	0.97/ 8 = 0.12 (1.22/ 8 = 0.15)	1.26/ 8 = 0.16 (1.50/ 8 = 0.19)	1.43/ 8 = 0.18 (1.66/ 8 = 0.21)	1.10/ 8 = 0.14 (1.34/ 8 = 0.17)
QGSJET-II-03	0.41/ 8 = 0.05 (0.52/ 8 = 0.07)	0.55/ 8 = 0.07 (0.67/ 8 = 0.08)	0.64/ 8 = 0.08 (0.76/ 8 = 0.10)	0.47/ 8 = 0.06 (0.58/ 8 = 0.07)
SIBYLL 2.1	10.6/ 8 = 1.33 (11.5/ 8 = 1.44)	11.1/ 8 = 1.39 (12.0/ 8 = 1.50)	11.4/ 8 = 1.42 (12.2/ 8 = 1.53)	10.8/ 8 = 1.35 (11.7/ 8 = 1.46)
IceCube-59 2015 [9], $10^2 < E_\nu \lesssim 10^6$ GeV, $90° < \theta < 180°$				
KM	4.79/10 = 0.48 (5.82/10 = 0.58)	4.49/10 = 0.45 (5.51/10 = 0.55)	4.40/10 = 0.44 (5.42/10 = 0.54)	4.64/10 = 0.46 (5.67/10 = 0.57)
QGSJET-II-03	3.58/10 = 0.36 (3.89/10 = 0.39)	3.15/10 = 0.32 (3.46/10 = 0.35)	3.00/10 = 0.30 (3.31/10 = 0.33)	3.38/10 = 0.34 (3.69/10 = 0.37)
SIBYLL 2.1	18.0/10 = 1.80 (18.8/10 = 1.88)	17.8/10 = 1.78 (18.6/10 = 1.86)	17.8/10 = 1.78 (18.6/10 = 1.86)	17.9/10 = 1.79 (18.7/10 = 1.87)
ANTARES 2021 [5], $10^2 < E_\nu \lesssim 5 \times 10^4$ GeV, $90° < \theta < 180°$				
KM	1.74/ 5 = 0.35 (1.72/ 5 = 0.34)	1.80/ 5 = 0.36 (1.76/ 5 = 0.35)	1.84/ 5 = 0.37 (1.79/ 5 = 0.36)	1.76/ 5 = 0.35 (1.74/ 5 = 0.35)
QGSJET-II-03	0.19/ 5 = 0.04 (0.12/ 5 = 0.02)	0.20/ 5 = 0.04 (0.11/ 5 = 0.02)	0.20/ 5 = 0.04 (0.10/ 5 = 0.02)	0.19/ 5 = 0.04 (0.12/ 5 = 0.02)
SIBYLL 2.1	20.0/ 5 = 4.00 (19.4/ 5 = 3.88)	20.2/ 5 = 4.04 (19.6/ 5 = 3.91)	20.4/ 5 = 4.08 (19.7/ 5 = 3.94)	20.1/ 5 = 4.02 (19.5/ 5 = 3.90)
ANTARES 2013 [4] & **ANTARES 2021** [5] $10^2 < E_\nu \lesssim 10^6$ GeV				
KM	6.20/15 = 0.41 (7.07/15 = 0.47)	6.03/15 = 0.40 (6.86/15 = 0.46)	5.96/15 = 0.40 (6.77/15 = 0.45)	6.11/15 = 0.41 (6.98/15 = 0.47)
QGSJET-II-03	7.37/15 = 0.49 (8.31/15 = 0.55)	8.66/15 = 0.58 (8.02/15 = 0.53)	6.97/15 = 0.46 (7.87/15 = 0.52)	7.24/15 = 0.48 (8.18/15 = 0.55)
SIBYLL 2.1	21.6/15 = 1.44 (21.8/15 = 1.45)	21.6/15 = 1.44 (21.8/15 = 1.45)	21.8/15 = 1.45 (21.8/15 = 1.45)	21.6/15 = 1.44 (21.8/15 = 1.45)
Combined data [1, 3–6, 9, 12] $E_\nu \lesssim 10^6$ GeV				
KM	39.1/54 = 0.72 (49.8/54 = 0.92)	37.8/54 = 0.70 (48.2/54 = 0.89)	37.3/54 = 0.69 (47.6/54 = 0.88)	38.5/54 = 0.71 (49.0/54 = 0.91)
QGSJET-II-03	47.2/50 = 0.94 (56.4/50 = 1.13)	47.0/50 = 0.94 (54.4/50 = 1.09)	44.5/50 = 0.89 (53.6/50 = 1.07)	46.4/50 = 0.93 (55.5/50 = 1.11)
SIBYLL 2.1	67.6/50 = 1.35 (73.5/50 = 1.47)	67.1/50 = 1.34 (72.8/50 = 1.46)	67.2/50 = 1.34 (72.7/50 = 1.45)	67.3/50 = 1.35 (73.2/50 = 1.46)

(ndf = 10, 11)).

In the analysis of Super-Kamiokande data [12] we use only 4 (ν_μ) and 2 (ν_e) data points measured at high energies. We consider high energy models QGSJET-II-03 and SIBYLL 2.1 as reasonable ones at energies $E_\nu \geq 100$ GeV, while KM is valid in the wider energy range,

$E_\nu \geq 10$ GeV. Thus, we compare the KM-predicted ν_μ spectrum (ndf = 4) and that of other theoretical models (ndf = 2) with measured ones in Fréjus 1995 [1] and Super-Kamiokande [12] at neutrino energies above 10 GeV. The same relates to four and three points of the ν_e flux measured in the IceCube [7].

Table III: $\chi^2/$ndf values calculated for the measured and predicted ν_e spectra.

Experiment, CN | PN models	χ^2 (CN)	χ^2 (CN+PN) QGSM	SIBYLL 2.3c	BEJKRSS
Super-Kamiokande I–IV 2016 [12], $E_\nu < 100$ GeV, $90^\circ < \theta < 180^\circ$				
KM		8.44/ 2 = 4.22 (7.21/ 2 = 3.61)		
IceCube-79 DeepCore-13 2013 [7], $10 < E_\nu \lesssim 10^5$ GeV, $90^\circ < \theta < 180^\circ$				
KM	22.5/ 4 = 5.63 (24.9/ 4 = 6.23)	22.4/ 4 = 5.60 (24.8/ 4 = 6.20)	22.4/ 4 = 5.60 (24.8/ 4 = 6.20)	22.5/ 4 = 5.63 (24.9/ 4 = 6.23)
QGSJET-II-03	1.11/ 3 = 0.37 (1.18/ 3 = 0.39)	1.01/ 3 = 0.34 (1.08/ 3 = 0.36)	0.95/ 3 = 0.32 (1.01/ 3 = 0.34)	1.07/ 3 = 0.36 (1.14/ 3 = 0.38)
SIBYLL 2.1	0.68/ 3 = 0.23 (0.82/ 3 = 0.27)	0.60/ 3 = 0.20 (0.74/ 3 = 0.25)	0.57/ 3 = 0.19 (0.71/ 3 = 0.24)	0.65/ 3 = 0.22 (0.78/ 3 = 0.26)
IceCube-86 DeepCore-8 2015 [10], $10^2 < E_\nu \lesssim 10^5$ GeV, $90^\circ < \theta < 180^\circ$				
KM	5.82/ 4 = 1.46 (5.98/ 4 = 1.50)	5.47/ 4 = 1.37 (5.58/ 4 = 1.40)	5.23/ 4 = 1.31 (5.35/ 4 = 1.34)	5.65/ 4 = 1.41 (5.79/ 4 = 1.45)
QGSJET-II-03	4.81/ 4 = 1.20 (5.14/ 4 = 1.29)	4.60/ 4 = 1.15 (4.86/ 4 = 1.22)	4.48/ 4 = 1.12 (4.72/ 4 = 1.18)	4.70/ 4 = 1.17 (5.00/ 4 = 1.25)
SIBYLL 2.1	8.70/ 4 = 2.17 (9.39/ 4 = 2.35)	8.88/ 4 = 2.22 (9.49/ 4 = 2.37)	9.12/ 4 = 2.28 (9.71/ 4 = 2.43)	8.74/ 4 = 2.19 (9.40/ 4 = 2.35)
ANTARES 2021 [5], $10^2 < E_\nu \lesssim 5 \times 10^4$ GeV, $90^\circ < \theta < 180^\circ$				
KM	10.5/ 3 = 3.50 (11.2/ 3 = 3.73)	12.4/ 3 = 4.14 (12.8/ 3 = 4.27)	14.0/ 3 = 4.67 (14.3/ 3 = 4.75)	11.2/ 3 = 3.73 (11.8/ 3 = 3.93)
QGSJET-II-03	13.8/ 3 = 4.60 (13.5/ 3 = 4.50)	16.2/ 3 = 5.41 (15.6/ 3 = 5.18)	18.2/ 3 = 6.05 (17.3/ 3 = 5.75)	14.8/ 3 = 4.93 (14.3/ 3 = 4.77)
SIBYLL 2.1	40.1/ 3 = 13.4 (40.0/ 3 = 13.3)	43.8/ 3 = 14.6 (43.2/ 3 = 14.4)	46.6/ 3 = 15.5 (45.8/ 3 = 15.3)	41.6/ 3 = 13.7 (41.3/ 3 = 13.8)
Combined data: IceCube [7, 10] & **ANTARES 2021** [5], $10 < E_\nu \lesssim 10^5$ GeV, $90^\circ < \theta < 180^\circ$				
KM	38.8/11 = 3.53 (42.1/11 = 3.83)	40.3/11 = 3.66 (43.2/11 = 3.93)	41.6/11 = 3.78 (44.5/11 = 4.05)	39.4/11 = 3.58 (42.5/11 = 3.86)
QGSJET-II-03	19.7/10 = 1.97 (19.8/10 = 1.98)	21.8/10 = 2.18 (21.5/10 = 2.15)	23.6/10 = 2.36 (23.0/10 = 2.30)	20.6/10 = 2.06 (20.4/10 = 2.04)
SIBYLL 2.1	49.5/10 = 4.95 (50.2/10 = 5.02)	53.3/10 = 5.33 (53.4/10 = 5.34)	56.3/10 = 5.63 (56.2/10 = 5.62)	51.0/10 = 5.10 (51.5/10 = 5.15)

The χ^2 values obtained with KM are QGSJET-II are closely related for all data, differing from those for SIBYLL 2.1. QGSJET-II and KM give the best fit of the IceCube-40 data [6], while the data obtained by Fréjus [1], AMANDA-II [3], ANTARES 2013 [4], and Super-Kamiokande [12] are better described with SIBYLL 2.1.

The PN fluxes were calculated using all listed charm production models, but only three of them, QGSM [24], SIBYLL 2.3c [40], and BEJKRSS [44], are presented in Tables I–III. As may be seen from these tables, the prompt neutrinos contribution is practically negligible for all measurements.

Table IV presents central values of the "crossing energy" (obtained with six charm production models) which dispersed in the range $0.8 - 4$ PeV. The "crossing energies" derived with QGSM [24], PROSA [41] and GM-VFNS [45] are almost coincident for KM (close to that for SIBYLL 2.3c [40]) and QGSJET-II-03 [31] taken separately. The GRRST [43] and BEJKRSS [44] predict highest "crossing energies".

The bulk analysis of conventional muon neutrino spectra shows that all flux models are consistent with measurements. However, SIBYLL 2.1 is in a tension with the IceCube-59 data for zenith angles $90^\circ < \theta < 120^\circ$ ($\chi^2/$ndf $\simeq 3.9$), as well as with the ANTARES 2021 ($\chi^2/$ndf $\simeq 4.0$) (Table II) – corresponding p values are $p \simeq 6 \times 10^{-5}$ (IceCube-59) and $p \simeq 10^{-3}$ (ANTARES 2021). While QGSJET-II and KM give $p = 0.87$ (QGSJET-II) and $p = 0.28$ (KM) for IceCube-59, as well $p = 0.999$ (QGSJET-II) and $p = 0.88$ (KM) for ANTARES 2021 data. Thus KM and QGSJET-II are in close agreement with the latest measurements of the atmospheric muon neutrino spectrum.

Opposite results were obtained for AMANDA-II: SIBYLL 2.1 appears as the preferred model ($p = 0.69$)

Table IV: Central values of the crossing energy (in PeV) predicted with the flux models.

CN	PN models	QGSM	SIBYLL 2.3c	PROSA	GM-VFNS	GRRST	BEJKRSS
KM	1.70	1.59	1.65	1.59	3.97	2.98
QGSJET-II-03	0.98	0.76	0.98	1.05	1.70	1.90
SIBYLL 2.1	1.55	1.20	1.55	1.48	3.47	2.75

Table V: Comparative significance of CN models used in the analysis of ν_μ spectra derived by IceCube-59 2015 (10 data points), and the combined data of ANTARES 2013 & ANTARES 2021 (15 data points). See Table II for details.

Experiment	CN models	QGSJET-II / KM	SIBYLL 2.1 / KM	SIBYLL 2.1 / QGSJET-II
IceCube-59 2015	$1.10\,\sigma$	$3.63\,\sigma$	$3.80\,\sigma$
ANTARES 2013 + ANTARES 2021	$1.07\,\sigma$	$3.92\,\sigma$	$3.77\,\sigma$

in comparison with KM ($p \simeq 0.01$) and QGSJET-II ($p \simeq 2 \times 10^{-4}$).

Notice also that close agreement of the SIBYLL 2.1 prediction ($p = 0.999$) with ANTARES 2013 data is ruined by ANTARES 2021 ($p = 1.2 \times 10^{-3}$), while KM and QGSJET-II-03 keep the accordance with the latter data ($p \approx 0.88 - 0.99$). Simialr results are obtained also for the combined data ANTARES 2013+2021: $p = 0.98$ (KM) and $p = 0.95$ (QGSJET-II) against $p = 0.12$ for SIBYLL 2.1 (Tables I and II).

The IceCube-59 2015 [9] data within the interval $90^{\rm o} < \theta < 120^{\rm o}$ are described by models KM, QGSJET-II, and SIBYLL 2.1 with a lower confidence level ($p = 0.28, 0.87, 6 \times 10^{-4}$) as compared with that for angles $120^{\rm o} < \theta < 180^{\rm o}$ ($p = 0.998, 0.999$, and 0.225). The discrepancy may result from an inaccuracy in analysis of events induced by neutrinos passing the detector near the horizon.

Our calculations showed that the zenith-angle cut influences moderately on the angle-averaged conventional neutrino flux: reducing the angle interval by $\sim 1^{\rm o}$ near the horizon leads to decrease in the spectra by $\sim 3\%$ for neutrino energies above 100 TeV.

Table V presents the comparative statistical significance of hadronic interactions models used in the analysis of ν_μ spectra derived in IceCube-59 (10 data points) [9] and in ANTARES experiments [4, 5] (15 points). This table demonstrates the proximity of the QGSJET-II-03 and Kimel & Mokhov predictions ($\sim 1\sigma$) relative to these experiments, while the SIBYLL 2.1 proves a certain tension with the data ($> 3.5\sigma$).

As regards to ν_e spectra, SIBYLL 2.1 and QGSJET-II-03 give a good description of IceCube-79 (with 3 data points involved in the analysis) [7]. The KM model gives similar result for the same data (3 points) but fails with $\chi^2/{\rm ndf} \simeq 5.6$ if all 4 points are included. Nevertheless KM and QGSJET-II-03 give fairly good fit for the IceCube-86 ν_e spectrum (4 points) [10]: $p \simeq 0.21$ (KM) and 0.31 (QGSJET-II).

Although, for reasons mentioned above, KM seems suitable for describing two of four ν_e data points (beyond 10 GeV) measured with Super-Kamiokande [12], actually the model hardly fits them ($p \simeq 1.5 \times 10^{-2}$).

The χ^2 analysis of the spectra measured in the IceCube-59 [9], IceCube-79 [7], and IceCube-86 [10] shows a slight preference of the H3a model for the cosmic ray spectrum as compared to the ZS parameterization.

VI. CONCLUSIONS

Predicted differential spectra of atmospheric muon neutrino successfully describe the experimental data within the experimental uncertainties. Both parameterizations of the cosmic rays spectrum, by Zatsepin & Sokolskaya and Hillas & Gaisser, produce close χ^2 values for the datasets under analysis, i.e. they are statistically undistinguished.

The calculated spectra of atmospheric muon neutrinos agree well with data obtained in Fréjus , AMANDA, IceCube, and ANTARES experiments. QGSJET-II-03 and KM lead to the best description of IceCube-59 data and ANTARES 2021 measurements of the ν_μ spectrum, SIBYLL 2.1 is a good model to describe the AMANDA-II and the ANTARES 2013 muon neutrino data. The Kimel & Mokhov model also provides suitable predictions for the IceCube-59 and ANTARES 2021, and the best one for combined data ANTARES 2013 + ANTARES 2021 ($p = 0.98$). The minimal χ^2 value for the total data on the ν_μ spectrum is also derived with Kimel & Mokhov model ($p = 0.94$).

As concerns atmospheric electron neutrinos, low event statistics in the measurements of the ν_e flux beyond 100 GeV impedes the unique choice of the preferred hadronic interactions model.

The statistical analysis shows that none of the discussed neutrino flux models leads to the statistically significant conrtibution of the prompt atmospheric neutri-

nos in the energy range covered by the neutrino telescopes.

Thus we can infer from the analysis that the high-energy atmospheric neutrino spectra calculated with the consistent scheme [19, 24–29] are sufficiently reliable and might be suitable for numerical simulation of the atmospheric neutrino events in the operating neutrino telescopes, as well as in the future experiments, Baikal-GVD [55–57], IceCube-Gen2 [58, 59], and KM3NeT/ORCA [60]. We expect that increased statistics on the muon, electron and tau neutrino events due to functional capabilities of the next generation of neutrino telescopes will enable one to solve the prompt neutrino problem.

[1] K. Daum *et al.* (Fréjus Collaboration), Determination of the atmospheric neutrino spectra with the Fréjus detector, Z. Phys. C **66**, 417 (1995).

[2] R. Abbasi *et al.* (IceCube Collaboration), Determination of the atmospheric neutrino flux and searches for new physics with AMANDA-II, Phys. Rev. D **79**, 102005 (2009) [arXiv:0902.0675].

[3] R. Abbasi *et al.* (IceCube Collaboration), The energy spectrum of atmospheric neutrinos between 2 and 200 TeV with the AMANDA-II detector, Astropart. Phys. **34**, 48 (2010) [arXiv:1004.2357].

[4] S. Adrian-Martinez *et al.* (ANTARES Collaboration), Measurement of the atmospheric ν_μ energy spectrum from 100 GeV to 200 TeV with the ANTARES telescope, Eur. Phys. J. C **73**, 2606 (2013) [arXiv:1308.1599].

[5] A. Albert *et al.* (ANTARES Collaboration), Measurement of the atmospheric ν_e and ν_μ energy spectra with the ANTARES neutrino telescope, Phys. Lett. B **816**, 136228 (2021) [arXiv:2101.12170].

[6] R. Abbasi *et al.* (IceCube Collaboration), Measurement of the atmospheric neutrino energy spectrum from 100 GeV to 400 TeV with IceCube, Phys. Rev. D **83**, 012001 (2011) [arXiv:1010.3980].

[7] M. G. Aartsen *et al.* (IceCube Collaboration), Measurement of the atmospheric ν_e flux in IceCube, Phys. Rev. Lett. **110**, 151105 (2013) [arXiv:1212.4760].

[8] M. G. Aartsen *et al.* (IceCube Collaboration)), Search for a diffuse flux of astrophysical muon neutrinos with the IceCube 59-string configuration, Phys. Rev. D **89**, 062007 (2014) [arXiv:1311.7048].

[9] M. G. Aartsen *et al.* (IceCube Collaboration), Development of a general analysis and unfolding scheme and its application to measure the energy spectrum of atmospheric neutrinos with IceCube, Eur. Phys. J. C **75**, 116 (2015) [arXiv:1409.4535].

[10] M. G. Aartsen *et al.* (IceCube Collaboration), Measurement of the atmospheric ν_e spectrum with IceCube, Phys. Rev. D **91**, 122004 (2015) [arXiv:1504.03753].

[11] M. G. Aartsen *et al.* (IceCube Collaboration), Measurement of the ν_μ energy spectrum with IceCube-79, Eur. Phys. J. C **77**, 692 (2017) [arXiv:1705.07780].

[12] E. Richard *et al.* (Super-Kamiokande Collaboration), Measurements of the atmospheric neutrino flux by Super-Kamiokande: energy spectra, geomagnetic effects, and solar modulation, Phys. Rev. D **94**, 052001 (2016)

[arXiv:1510.08127].

[13] G. D. Barr *et al.*, A three–dimensional calculation of atmospheric neutrinos, Phys. Rev. D **70**, 023006 (2004) [arXiv:astro-ph/0403630].

[14] M. Honda *et al.*, Calculation of atmospheric neutrino flux using the interaction model calibrated with atmospheric muon data, Phys. Rev. D **75**, 043006 (2007) [arXiv:astro-ph/0611418].

[15] M. Honda *et al.*, Improvement of low energy atmospheric neutrino flux calculation using the JAM nuclear interaction model, Phys. Rev. D **83**, 123001 (2011) [arXiv:1102.2688].

[16] V. A. Naumov, T. S. Sinegovskaya, Simple method for solving transport equations describing the propagation of cosmic ray nucleons in the atmosphere, Phys. Atom. Nucl. **63**, 1927 (2000).

[17] V. A. Naumov, T. S. Sinegovskaya, Atmospheric proton and neutron spectra at energies above 1-GeV, in *Proceedings of the 27th International Cosmic Ray Conference* (Hamburg, 2001), Vol. 1, p. 4173 [arXiv:hep-ph/0106015].

[18] A. A. Kochanov, T. S. Sinegovskaya, and S. I. Sinegovsky, High-energy cosmic ray fluxes in the Earth atmosphere: calculations vs experiments, Astropart. Phys. **30**, 219 (2008) [arXiv:0803.2943].

[19] T. S. Sinegovskaya, A. D. Morozova, and S. I. Sinegovsky, High-energy neutrino fluxes and flavor ratio in the Earth's atmosphere, Phys. Rev. D **91**, 063011 (2015) [arXiv:1407.3591].

[20] S. I. Sinegovsky *et al.*, Atmospheric muon flux at PeV energies, Int. J. Mod. Phys. A **25**, 3733 (2010).

[21] A. A. Kochanov, T. S. Sinegovskaya, and S. I. Sinegovsky, High-energy cosmic ray muons in the Earth's atmosphere, J. Exp. Theor. Phys. **116**, 395 (2013)

[22] A. A. Kochanov *et al.*, High-energy atmospheric muon flux calculations in comparison with recent measurements, J. Phys. Conf. Ser. **1181**, 012054 (2019) [arXiv:1907.00640].

[23] A. A. Kochanov *et al.*, Atmospheric neutrino spectra: a statistical analysis of calculations in comparison with experiment, Bull. Russ. Acad. Sci. Phys. **85**, 433 (2021).

[24] S. I. Sinegovsky and M. N. Sorokovikov, Prompt atmospheric neutrinos in the quark–gluon string model, Eur. Phys. J. C **80**, 34 (2020) [arXiv:1812.11341].

[25] A. D. Morozova *et al.*, Calculation of atmospheric high-

energy neutrino spectra and the measurement data of IceCube and ANTARES experiments, Bull. Russ. Acad. Sci. Phys. **81**, 516 (2017).

[26] A. A. Kochanov *et al.*, Examination of calculations of the atmospheric muon and neutrino spectra using new measurements, Bull. Russ. Acad. Sci. Phys. **83**, 933 (2019).

[27] A. D. Morozova *et al.*, Influence of cosmic-ray spectrum and hadron–nucleus interaction model on the properties of high-energy atmospheric-neutrino fluxes, Phys. Atom. Nucl. **82**, 491 (2019).

[28] A. D. Morozova *et al.*, The comparison of the calculated atmospheric neutrino spectra with the measurements of IceCube and ANTARES experiments, J. Phys. Conf. Ser. **798**, 012101 (2017).

[29] A. D. Morozova *et al.*, Influence of hadronic interaction models on characteristics of the high-energy atmospheric neutrino flux, J. Phys. Conf. Ser. **934**, 012008 (2017).

[30] N. N. Kalmykov, S. S. Ostapchenko, and A. I. Pavlov, Quark-gluon string model and EAS simulation problems at ultra-high energies, Nucl. Phys. B (Proc. Suppl.) **52**, 17 (1997).

[31] S. Ostapchenko, QGSJET-II: Towards reliable description of very high energy hadronic interactions, Nucl. Phys. B (Proc. Suppl.) **151**, 143 (2006) [arXiv:hep-ph/0412332].

[32] S. Ostapchenko, Hadronic interactions at cosmic ray energies, Nucl. Phys. B (Proc. Suppl.) **175**–**176**, 73 (2008) [arXiv:hep-ph/0612068].

[33] E. J. Ahn *et al.*, Cosmic ray interaction event generator SIBYLL 2.1, Phys. Rev. D **80**, 094003 (2009) [arXiv:0906.4113].

[34] A. N. Kalinovsky, N. V. Mokhov, and Y. P. Nikitin, *Passage of high-energy particles through matter* (American Institute of Physics, New York, 1989).

[35] L. R. Kimel and N. V. Mokhov, Particle distributions in 10^{-2}—10^{12} eV energy range initiated by high-energy hadrons in dense media, Izv. Vuz. Fiz. **10**, 17 (1974).

[36] V. I. Zatsepin and N. V. Sokolskaya, Three component model of cosmic ray spectra from 100 GeV up to 100 PeV, Astron. Astrophys. **458**, 1 (2006) [arXiv:astro-ph/0601475].

[37] T. K. Gaisser, Spectrum of cosmic-ray nucleons, kaon production, and the atmospheric muon charge ratio, Astropart. Phys. **35**, 801 (2012) [arXiv:1111.6675].

[38] A. D. Panov *et al.*, Elemental energy spectra of cosmic rays from the data of the ATIC-2 experiment, Bull. Russ. Acad. Sci. Phys. **71**, 494 (2007) [arXiv:astro-ph/0612377]

[39] A. D. Panov *et al.*, Energy spectra of abundant nuclei of primary cosmic rays from the data of ATIC-2 experiment: final results, Bull. Russ. Acad. Sci. Phys. **73**, 564 (2009) [arXiv:1101.3246].

[40] A. Fedynitch *et al.*, Hadronic interaction model SIBYLL 2.3c and inclusive lepton fluxes, Phys. Rev. D **100**, 103018 (2019) [arXiv:1806.04140].

[41] O. Zenaiev *et al.* (PROSA Collaboration), Improved constraints on parton distributions using LHCb, ALICE and HERA heavy-flavour measurements and implications for the predictions for prompt atmospheric-neutrino fluxes, JHEP **04**, 118 (2020) [arXiv:1911.13164];

https://prosa.desy.de/Main_Page.

[42] M. V. Garzelli *et al.* (PROSA Collaboration), Prompt neutrino fluxes in the atmosphere with PROSA parton distribution functions, JHEP **05**, 004 (2017) [arXiv:1611.03815].

[43] R. Gauld *et al.*, The prompt atmospheric neutrino flux in the light of LHCb, JHEP **02**, 130 (2016) [arXiv:1511.06346].

[44] A. Bhattacharya *et al.*, Prompt atmospheric neutrino fluxes: perturbative QCD models and nuclear effects, JHEP **11**, 167 (2016) [arXiv:1607.00193].

[45] M. Benzke *et al.*, Prompt neutrinos from atmospheric charm in the general-mass variable-flavor-number scheme, JHEP **12**, 021 (2017) [arXiv:1705.10386].

[46] A. B. Kaidalov and O. I. Piskunova, Production of charmed particles in the quark - gluon string model, Sov. J. Nucl. Phys. **43**, 994 (1986).

[47] A. B. Kaidalov, High-energy hadronic interactions (20 years of the quark gluon strings model), Phys. Atom. Nucl. **66**, 1994 (2003).

[48] E. V. Bugaev *et al.*, Prompt leptons in cosmic rays, Nuovo Cim. C **12**, (1989).

[49] E. V. Bugaev *et al.*, Atmospheric muon flux at sea level, underground and underwater, Phys.Rev. D **58**, 054001 (1998).

[50] V. A. Naumov, T. S. Sinegovskaya, and S. I. Sinegovsky, The $K_{\ell 3}$ form factors and atmospheric neutrino ratio at high energies, Nuovo Cim. A **111**, 129 (1998).

[51] A. Fedynitch *et al.*, MCE_Q – numerical code for inclusive lepton flux calculations, PoS (ICRC 2015) 1129.

[52] A. Fedynitch, Phenomenology of atmospheric neutrinos, EPJ Web Conf. **116**, 11010 (2016).

[53] G. Cowan *et al.* Asymptotic formulae for likelihood-based tests of new physics, Eur. Phys. J. C **71**, 1554 (2011).

[54] M. Tanabashi *et al.* (Particle Data Group), Review of Particle Physics, Phys. Rev. D **98**, 030001 (2018).

[55] I. Belolaptikov and Zh.-A. Dzhilkibaev on behalf of the Baikal-GVD Collaboration, Neutrino telescope in Lake Baikal: Present and nearest future, PoS (ICRC2021) 002.

[56] A. V. Avrorin *et al.* High-energy neutrino follow-up at the Baikal–GVD neutrino telescope, Astronomy Lett. **47**, 94 (2021).

[57] J. Stasielak, P. Malecki, D. Naumov *et al.* on behalf of the Baikal-GVD Collaboration, High-energy neutrino astronomy – Baikal-GVD neutrino telescope in Lake Baikal, Symmetry **13**, 377 (2021).

[58] M. G. Aartsen *et al.* (IceCube-Gen2 Collaboration), IceCube-Gen2: the window to the extreme Universe, J. Phys. G: Nucl. Part. Phys. **48**, 060501 (2021) [arXiv:2008.04323].

[59] A. Ishihara *et al.*(IceCube Collaboration), The IceCube upgrade - design and science goals, PoS (ICRC2019) 1031 [arXiv:1908.09441].

[60] S. Adrián-Martínez *et al.* (KM3NeT Collaboration), KM3NeT 2.0 – Letter of intent for ARCA and ORCA, J. Phys. G: Nucl. Part. Phys. **43**, 084001 (2016) [arXiv:1601.07459].